David Merker[1,*]
Lutz Böhm[1]
Martin Oßberger[2]
Peter Klüfers[2]
Matthias Kraume[1]

Mass Transfer in Reactive Bubbly Flows – A Single-Bubble Study

The design of reactors with a dispersed gas in a liquid phase, e.g., bubble columns, is often based on rather roughly estimated parameters. To obtain a better understanding of the influence and interaction of the fluid dynamics and the mass transfer in the presence of a chemical reaction of NO and Fe(EDTA) in the liquid phase, the complex system of a bubbly flow is here reduced to single-bubble investigations. For this purpose, mass transfer is investigated with and without chemical reaction to be able to differentiate between various influencing factors and determined enhancement caused by the chemical reaction. Two experimental setups are applied, namely, the first one with two moving cameras where the velocity is adapted to the rising velocity of the bubble, and the second one is a countercurrent-flow cell.

Keywords: Keywords: CO_2 mass transfer, Fe(NO), Gas-liquid system, Mass transfer enhancement, Reactive bubbly flow

Received: December 12, 2016; *revised:* March 02, 2017; *accepted:* March 10, 2017

DOI: 10.1002/ceat.201600715

1 Introduction

Single-particle approaches are extensively investigated as they are utilized as a basis for complex multiple-particle systems. Particle swarms are widely found in process engineering applications such as bubble columns, moving-bed reactors or extraction columns. These are mentioned here as three exemplary unit operations with gaseous, solid, and liquid particulate phases. This work focuses on gas-liquid systems with gas as the particulate and liquid as the continuous phase and especially the mass transfer from the bubble to the liquid.

The common approach to this topic is to analyze the mass transfer coefficient on the liquid side $k_{A,L}$[1)]. In the dimensionless way it is represented for the given case as Sherwood number:

$$Sh = \frac{k_{A,L} d}{D_{A,L}} \tag{1}$$

with the equivalent bubble diameter d and the diffusion coefficient in the liquid $D_{A,L}$. This allows a calculation of the actual mass transfer of the absorption process:

$$\dot{N}_A = k_{A,L} A_{int} \left(c_{A,L,int} - c_{A,L,bulk}\right) = D_{A,L} A_{int} \left(\frac{\partial c_A}{\partial r}\right)_{L,int} \tag{2}$$

with A_{int} as the interfacial area, $c_{A,L,int}$ as the concentration on the liquid side on the interface, $c_{A,L,bulk}$ as the concentration in the liquid bulk, and r as the radial component. The concentration on the interface on the liquid side provides the link to the conditions on the gas side as the interfacial concentrations on both sides are connected with a solubility constant, e.g., described by Henry's law:

$$H_A RT \frac{c_{A,L,int}}{c_{tot,L}} = p \frac{c_{A,G,int}}{c_{tot,G}} \tag{3}$$

with H_A as the Henry's law solubility constants, $c_{tot,L}$ as the total concentration of all components of the liquid phase, $c_{A,G,int}$ as the concentration of component A on the interface of the gas side, $c_{tot,G}$ as the total concentration of all components of the gas phase, and p as the pressure. It can be assumed that in most cases the diffusion coefficient in the gas phase is larger than in the liquid phase by at least three orders of magnitude. Hence, the discussion of the mass transfer coefficient on the liquid side is often of main interest as the largest resistance for the total mass transfer lies on the liquid side. Assuming, the bubble shape and the velocity field around the bubble is known, analytically or numerically a concentration field can be calculated which can be used to determine a local and averaged mass transfer coefficient and, therefore, a local and an averaged Sherwood number can be calculated [1, 2]. This leads, e.g., to

1) List of symbols at the end of the paper.

[1]David Merker, Dr.-Ing. Lutz Böhm, Prof. Dr.-Ing. Matthias Kraume
david.merker@tu-berlin.de
Technische Universität Berlin, Chair of Chemical and Process Engineering, Sekr. FH 6-1, Strasse des 17. Juni 135, 10623 Berlin, Germany.

[2]Dr. Martin Oßberger, Prof. Dr. Peter Klüfers
Ludwig-Maximilians-Universität München, Chair of Inorganic Chemistry, Butenandtstrasse 5–13, Haus D, 81377 München, Germany.

the widely known case for a resting system without flows, described by a Reynolds number:

$$Re = \frac{vd}{\mu_L} = 0 \tag{4}$$

with v as the bubble rise velocity and μ_L as the dynamic viscosity of the liquid which leads to $Sh = 2$. Once the bubble is deformed in an unknown way and/or the velocity field is unknown, only empirical equations mostly of the type

$$Sh = 2 + f(Re,\ Sc) \tag{5}$$

with the Schmidt number

$$Sc_A = \frac{\nu_L}{D_{A,L}} = \frac{Pe_A}{Re} \tag{6}$$

where Pe_A is the Péclet number, can be found. These equations sometimes also depend on the ratio of the viscosities in the dispersed and the continuous phase, marking the fact that these equations are usually generally valid for systems with fluid particles, including drops or bubbles, and the excentricity.

Mersmann [2] found the empirical equation for spherical particles:

$$Sh = f\frac{2}{\sqrt{\pi}}\ Pe^{1/2} \tag{7}$$

with f as dimensionless factor depending on the Reynolds number. Brauer [3] developed another equation for oscillating particles:

$$Sh = 2 + 0.015 Re^{0.89} Sc_A^{0.7} \tag{8}$$

All equations are valid for bubbles rising in unconfined geometries. Concerning the influence of confining walls on the mass transfer, see, e.g., Hosoda et al. [4]. As an alternative, relations of the Sherwood number and the oscillation frequency can be found [5], such as:

$$Sh = 1.2\ (Pe_A\ Sr)^{1/2} \tag{9}$$

with the Strouhal number Sr defined as:

$$Sr = \frac{f_B d}{v} \tag{10}$$

with f_B as the rising path oscillation frequency.

Up to here, fairly simple cases were discussed. A steady state was assumed which neglects, e.g., that due to the mass transfer from the bubble to the liquid phase the bubble size and, therefore, the rise velocity, shape, and rise behavior changes during its ascent. This obviously has an influence on Re and Sh. For simplified cases with constant spherical bubble sizes but unsteady mass transfer, being valid for many liquid-liquid cases, due to a developing flow field results can be found for Sh numbers over the Fourier number:

$$Fo_A = \frac{4tD_{A,L}}{d^2} \tag{11}$$

with t as the time [6]. The results lie between the well-known behavior described by Higbie's penetration theory [7] with:

$$Sh = \frac{4}{\sqrt{\pi\ Fo}} \tag{12}$$

for small Fourier numbers and the exemplary result shown earlier for steady state for larger Fourier numbers.

The mass transfer process, which is of interest in this study, exhibits particular complexity. It combines a transient bubble ascent, including acceleration, oscillation in shape and rising path, size change, an overlaying countercurrent mass transfer due to unavoidable desorption (as discussed later) and additionally a homogeneous reaction in the liquid with the transferred component as one reactant. In cases with reaction, enhancement factors

$$E = \frac{k_{A,L,\ rea}}{k_{A,L}} \tag{13}$$

with $k_{A,L,rea}$ as the mass transfer coefficient with homogeneous reaction are defined.

In theory, the change of the concentration of component A would be described with the balance equation:

Case 1: Mass transfer gas (G) to liquid (L) of a pure gas

$$\frac{\partial N_{A,G}}{\partial t} = \frac{\partial\left(Vc_{A,G}\right)}{\partial t} = c_{A,G}\frac{\partial V}{\partial t} = -\dot{N}_{A,L} = -k_{A,L}A_{int}\left(c_{A,L,int} - c_{A,L,bulk}\right) = -k_{A,L}A_{int}\frac{p}{H_A}c_{tot,L} \tag{14}$$

with the assumption: the bubble only consists of component A, only absorption of A in liquid occurring, no A in liquid bulk. The amount of component A dissolved in the continuous phase during the single-bubble experiments changes the concentration in the bulk only very slightly. The mass transfer coefficient can be calculated as:

$$k_{A,L} = \frac{c_{A,G}}{c_{tot,L}}\frac{H_A}{p}\frac{\left(-\frac{\partial V}{\partial t}\right)}{A_{int}} \tag{15}$$

However, a countercurrent mass transfer from gas to liquid (component A) and liquid to gas (component B) takes place, resulting for the individual components in the following balance equations.

Case 2: Mass transfer gas to liquid (A) and liquid to gas (B) due to the low concentration of B, no interaction of the two countercurrent mass transfers is taken into account.

$$\frac{\partial N_{A,G}}{\partial t} = \frac{\partial\left(Vc_{A,G}\right)}{\partial t} = \dot{N}_{A,G} = -k_{A,L}A_{int}\left(c_{A,L,int} - c_{A,L,bulk}\right) = -k_{A,L}A_{int}\frac{p}{H_A}\frac{c_{A,G,int}}{c_{tot,G}}c_{tot,L,bulk} \tag{16}$$

and

$$\frac{\partial N_{B,G}}{\partial t} = \frac{\partial\left(Vc_{B,G}\right)}{\partial t} = \dot{N}_{B,L} = -k_{B,L}A_{int}\left(c_{B,L,int} - c_{B,L,bulk}\right) = -k_{B,L}A_{int}\left(\frac{p}{H_B}\frac{c_{B,G,int}}{c_{tot,G}}c_{tot,L} - c_{B,L,bulk}\right) \tag{17}$$

results in:

$$\frac{\partial\left(V\left[c_{A,G}+c_{B,G}\right]\right)}{\partial t}= -k_L A_{int}\left(p\frac{c_{tot,L}}{c_{tot,G}}\left[\frac{c_{B,G,int}}{H_B}-\frac{c_{A,G,int}}{H_A}\right]-c_{B,L,bulk}\right) \quad (18)$$

Since fluid dynamics, mass transfer, and chemical reaction influence each other, it is necessary to measure the individual effects and to describe their interactions. To achieve that goal, several values in high precision have to be measured during the ascent of a bubble. In literature, measurements are often missing the accuracy which is needed to derive the mass transfer of single bubbles in reactive systems. Furthermore, the influence of dissolved gases in the liquid phase has to be considered.

2 Materials and Methods

Experiments are performed in two setups to carry out mass transfer measurements with single bubbles. For short contact times, a setup can be used in which a bubble rises through a stagnant liquid. In this case, the observation time is limited by the height of the column in combination with the rising velocity of the bubble. By using a countercurrent-flow cell, a bubble can be examined as long as desired. Due to the used chemical systems, it was necessary to build both test cells in such a way that the liquid phase is only in contact with glass, polytetrafluoroethylene, and stainless steel.

2.1 Rising-Bubble Test Cell

To investigate the influence of fluid dynamics and chemical reactions on the mass transfer in bubbly flows more closely, a rising-bubble test cell was constructed. The setup is schematically presented in Fig. 1. It consists of a glass tube with a height of 2 m and an internal diameter of 75 mm. To provide better optical access to the column, a rectangular acrylic glass jacket is built around the glass tube (Fig. 1, No. 3). To control the temperature of the continuous liquid phase, a thermostat pumps water at $T = 25\,°C$ through the jacket (Fig. 1, No. 8). At the bottom of the column, single gas bubbles are generated at a glass capillary by using a syringe pump (Hamilton® PSD/2) (Fig. 1, No. 1). The size of the bubble can be varied by changing the capillary to one with another inner diameter (Fig. 1, No. 2).

Two high-speed cameras (Vieworks VC-4MC-M180E0-CM) with a resolution of $1200\times2048\,px^2$ at 250 fps and telecentric lenses (Sill TZM 2298) are attached on a vertical traverse system and rectangular to each other (Fig. 1, Nos. 4 and 5). The visible area of each camera is approximately $24\times40\,mm^2$. Opposite to each camera, light-emitting diode (LED) panels are used as backlight illumination for the shadowgraphy (Fig. 1, No. 7). The velocity of the traverse system is controlled with a National Instruments LabVIEW in real time by the relative bubble position in the current image of one of the cameras (Fig. 1, No. 6). Thus, the bubble can be kept over time steadily on any vertical position in the image.

Due to the two cameras moving on the traverse system, the bubble volume, shape, velocity, and trajectory can be measured in three dimensions during the whole ascent. The column is closed at the top and it is possible to work under a protective atmosphere (Fig. 1, No. 10). Hence, it is possible to measure systems which have to be free of, e.g., oxygen. One advantage of this design is having a stagnant fluid, whereby the bubble does not experience a superimposed velocity profile due to a movement of the continuous phase.

2.2 Countercurrent-Flow Cell

To make slow mass transfer effects ascertainable, longer measuring times are necessary. The countercurrent-flow cell can be applied to achieve long contact times with a small quantity of

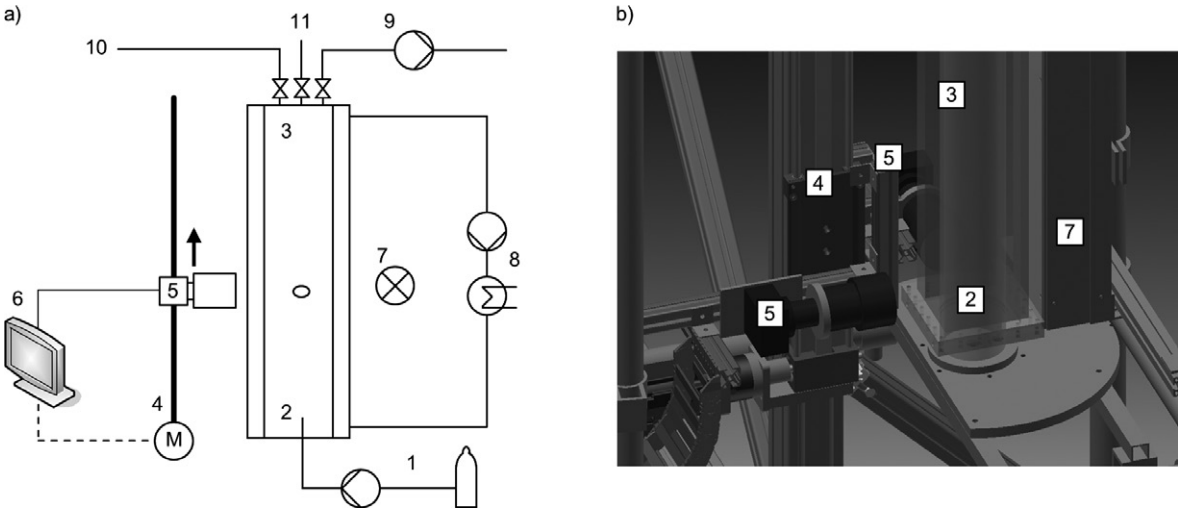

Figure 1. Experimental setup rising bubble test cell; (a) schematic sketch; (b) detail of the construction drawing; (1) syringe pump with gas source, (2) capillary, (3) column with jacket, (4) traverse system, (5) two cameras, (6) computer, (7) LED panel, (8) thermostat, (9) vacuum pump, (10) protective gas, (11) outlet.

liquid. Less than 200 mL of continuous phase is required. The schematic setup is shown in Fig. 2 a. A bubble is produced at the bottom of the glass cone (Fig. 2, No. 2) by a syringe pump. The bubble size and position is captured by a camera (The Imaging Source DMK 31BU03.H) with a resolution of $300 \times 1024\ px^2$ at 30 fps and telecentric lenses (Sill S5LPJ0202) (Fig. 2, No. 5). In this case, the camera is fixed and the bubble is held in the glass cone by a countercurrent-flow of the liquid. It is possible to fix a large spectrum of bubble sizes in the glass cone. An image analysis was implemented in National Instruments LabVIEW which determines the vertical position in the image in real time and controls the volumetric liquid flow accordingly through the gear pump (Fig. 2, No. 4) to keep the bubble at a fixed position in the image. Exemplary CO_2 bubbles with different shapes and volumes are displayed in Fig. 2 b. The volume of the bubble is approximated by the shape of a rotationally symmetrical ellipsoid.

2.3 Investigated Liquids and Gases

For the measurements, different chemical systems have been applied to measure and validate different effects. The fluid dynamics of air bubbles in water was investigated numerous times making this a feasible reference system. To be able to evaluate the mass transfer of gas bubbles, the volume reduction of CO_2 and NO bubbles in water was measured. The pure gaseous phases CO_2 and NO were studied as well as air. The liquid phase in all cases was ultrapure water with a conductivity of $0.055\ \mu S\ cm^{-1}$ at a constant temperature of 25 °C. In a following step, a chemical reaction system was used which consumed a gas component dissolved in the liquid as an educt.

Reactive system $Fe^{II}(NO)$: NO is well-known for its toxic properties but it has also important functions in the human body, like influencing the regulation of blood pressure [8]. In 1998, the Nobel Prize for Medicine or Physiology was awarded to Ignarro [9] who investigated the influence of $Fe^{II}(NO)$ compounds on the opening of the blood vessels. As a result, more studies on the Fe(NO) compounds and their activity and properties have been carried out, e.g., by Franke and van Eldik [10].

However, the formation of gaseous NO exhibits a major challenge in the combustion of fossil fuels. There exist different possibilities to clean the exhaust gases. One approach is known as the BioDeNOx technology where NO binds to an aqueous $Fe^{II}(EDTA)$ compound. The absorbed NO is subsequently reduced in a bioreactor by bacteria. This cost-effective and "green" NO removal technology has claimed several current publications [11–20].

The fundamental reaction of the absorption of NO by ferrous solutions follows the scheme:

$$Fe^{2+}{}_{aq} + NO_g \rightleftharpoons [Fe(NO)]^{2+}{}_{aq} \tag{19}$$

In more detail, realizing water as a ligand, NO replaces one water molecule:

$$[Fe(H_2O)_6]^{2+} + NO \rightleftharpoons [Fe(H_2O)_5(NO)]^{2+} + H_2O \tag{20}$$

The selection of chelate ligands of the aminecarboxylato group has a strong influence on the reaction rate and the equilibrium constant as shown by Schneppensieper et al. [21]. Adding the well-known ligand EDTA with its potential six metal binding sites to the aqueous ferrous solution subsequently initiating NO to the solution results in a very stable complex of $[Fe(EDTA)(NO)]^{2-}$:

$$[Fe(H_2O)_6]^{2+} + EDTA^{4-} \rightleftharpoons [Fe(H_2O)(EDTA)]^{2-} + 5\ H_2O \tag{21}$$

$$[Fe(H_2O)(EDTA)]^{2-} + NO \rightleftharpoons [Fe(EDTA)(NO)]^{2-} + H_2O \tag{22}$$

Comparing the stability constant of $[Fe(EDTA)(NO)]^{2-}$ ($K_{NO} = (2.1 \pm 0.2) \times 10^6\ M^{-1}$) with that of $[Fe(H_2O)_5(NO)]^{2+}$ ($K_{NO} = (1.2 \pm 0.2) \times 10^3\ M^{-1}$) [22, 23], the stability effect of the

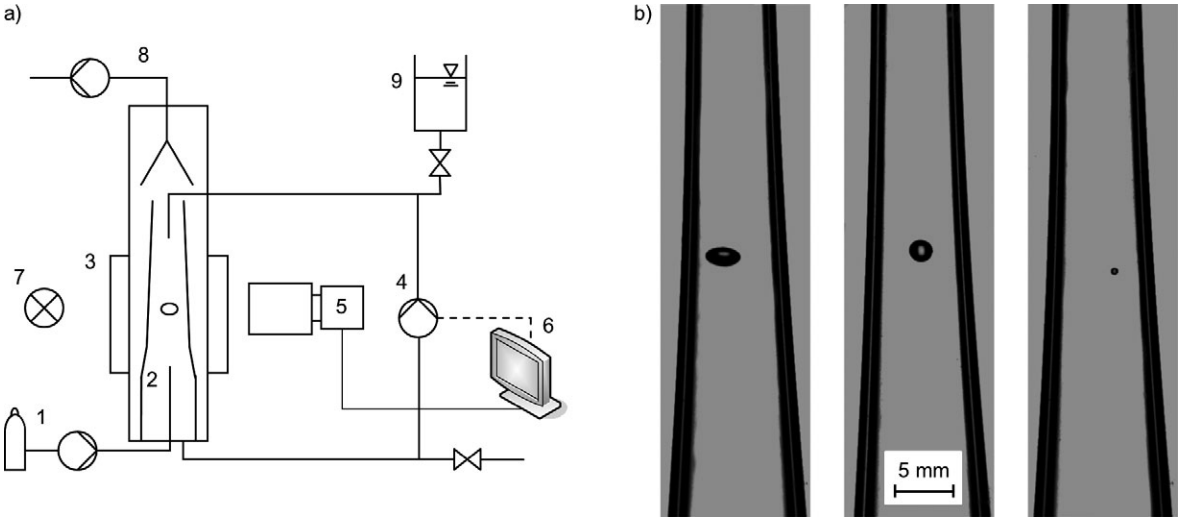

Figure 2. Experimental setup countercurrent-flow test cell; (a) schematic sketch; (b) differently sized bubbles kept on the same height in the glass cone by adjusted liquid volume flow; (1) syringe pump with gas source, (2) capillary, (3) glass cone with jacket, (4) pump, (5) camera, (6) computer, (7) light source, (8) glass funnel and syringe pump, (9) liquid phase.

chelate ligand is obvious. However, the stability of the Fe^{II}(Ligand)-NO system is not fully understood since the exact mechanism of the product formation and the rules of the relationship of structure and feature are, to our knowledge, still unknown. With two publications, the research group of Klüfers tries to fill this gap [24, 25].

In this work, all experiments were performed with EDTA and with degassed water to minimize the mass transfer from the liquid to the gas phase. Thus, water was boiled under an argon atmosphere because the solubility of gases decreases with increasing temperature. The boiled water was rapidly cooled to 25 °C with the aid of a cooling coil. For the preparation of the test system Fe^{II}(EDTA), powdery iron(II)sulfate heptahydrate (Sigma-Aldrich, CAS: 7782-63-0) and 1.1 equimolar ethylenediaminetetraacetic acid tetra-sodium salt hydrate (Sigma-Aldrich, CAS: 194491-31-1) were dissolved in water. The starting solution is colorless to slightly yellowish whereas the product Fe^{II}(Ligand)–NO is orange-brown. This colored product can be detected around the bubble and in the wake. The material properties used for the calculation are summarized in Tab. 1.

Table 1. Properties of the used systems.

Water as solvent	Henry's law solubility constants	Diffusivity
Combined with	H [mol m^{-3}Pa^{-1}]	D [m^{2}s^{-1}]
CO_2	3.3×10^{-4} [26]	1.92×10^{-9} [27]
NO	1.9×10^{-5} [26]	2.21×10^{-9} [28]

3 Results

To evaluate the effects of fluid dynamics, mass transfer, and the influence of a chemical reaction, the effects were analyzed individually.

3.1 Fluid Dynamics of the Reference System Air/Water

In the area of fluid dynamics of freely ascending bubbles without material transport and chemical reaction in water, many investigations have already been carried out, e.g., assembled in the overview of Clift et al. [1]. Such experiments can be used to proof the functionality of the developed measurement technique. The test system air/water was chosen as it does not show any mass transfer effects assuming that the water was in contact with air for a sufficient time before. The vertical rise velocity is sensitive to impurities since small amounts of impurities can have a significant influence on the behavior of the interface. The rising bubble test cell was used to record the bubble shape, volume, surface area, and the position in the 3D space. Fig. 3 a shows the helical rising trajectory of a bubble with an equivalent diameter of 2 mm, i.e., the diameter of a spherical bubble with the according measured bubble volume. By evaluating the displacement of the bubble between two pictures taken during the ascent, it is possible to determine the rise velocity at every point of the helical rising path.

The terminal rise velocities in ultrapure water for different bubble diameters without mass transfer are illustrated in Fig. 3 b. The results are reproducible and the standard deviation for a measurement was less than 3 %. The velocities are in good agreement with values found in literature [1] for pure water and, thus, a free-moving interface. Therefore, it can be stated that working in an impurity-free environment is possible in the rig, and the measurement technique with the controlled traverse system allows a precise measurement. If components of the reactive system Fe^{II}(EDTA)-NO mentioned in Sect. 2.3 are added, the terminal velocities change significantly.

The velocities were measured with bubbles without mass transfer. The measurements of mass transfer will be discussed in Sect. 3.3. The lower velocity limit is the case of a fully contaminated system in which interfacial active substances (surfac-

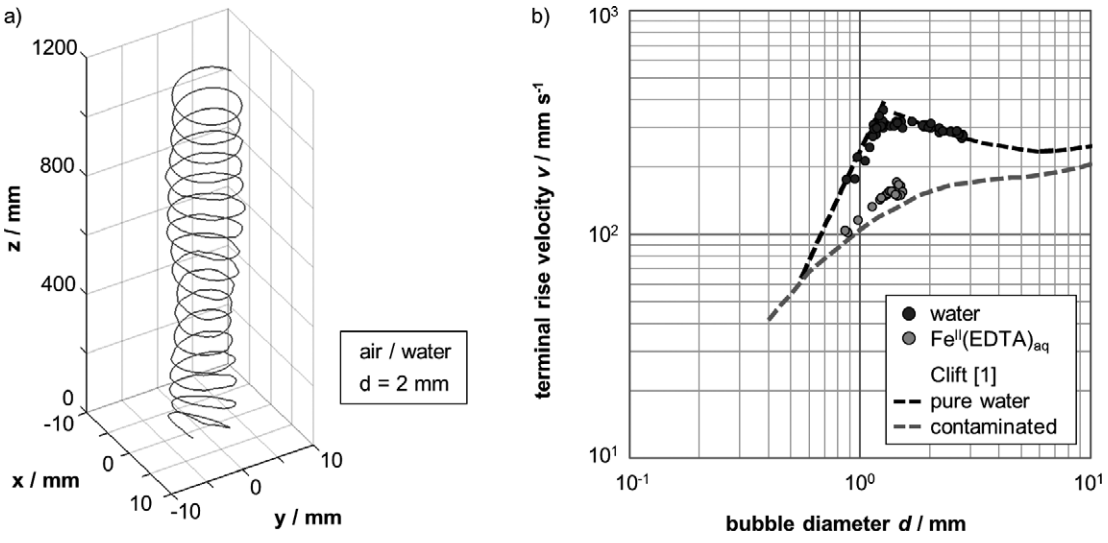

Figure 3. (a) Helical trajectory of an air bubble with $d = 2$ mm in water reconstructed from the images of two cameras positioned at right angles to each other. (b) Terminal rise velocity of bubbles in pure water and water containing $c_{Fe^{II}(EDTA)} = 75$ mmol L^{-1} compared with equations published by Clift [1].

tants) adsorb on the interface and thus, the rate of ascent of the bubble is reduced due to a hardened interface as shown by the gray dashed line. The terminal rise velocities of bubbles in a solution of $Fe^{II}(EDTA)_{aq}$ with a concentration of 75 mmol L^{-1} are close to those achieved in totally contaminated systems. The interface is not freely movable due to contamination with the components of the reactive system, which are acting as surfactants.

3.2 Reference Measurements for Mass Transfer

To measure the mass transfer between a gas bubble and a liquid continuous phase accurately, the pretreatment of the water phase is of crucial importance. Fig. 4 a presents results from the countercurrent-flow cell for measurements with similar initial bubble volumes and differently prepared aqueous phases. Pure CO_2 bubbles were generated and within a few seconds a large part of the gas phase was transferred into the liquid phase. The flow rate was adjusted to the changing fluid dynamics of the shrinking bubble. In the case of untreated pure water, approximately 50 % of the gas volume remained in steady state. Ultrapure water stripped with nitrogen (N_2) and degassed ultrapure water (reached by cooking the water for 60 min), respectively, showed smaller remaining volumes. Degassed water reaches bubble volume values close to zero. After approximately 2 min only less than 1 % of the initial volume was present in the residual bubble. The transient volume development of a NO bubble in degassed water is given in Fig. 4 a as well. As expected, the mass transfer of NO into the gas phase is slower compared to CO_2. This is due to the lower solubility in water.

From the measurements with differently prepared water it is obvious that not only the transport of mass from the bubble into the liquid has to be taken into account. The influence of the countercurrent mass transfer from the liquid phase into the gas phase has to be considered since that transfer can change the evaluation of the occurring mass transfer coefficients for the gas phase drastically. In the case of measurements with shorter ascent paths or contact times, this effect will not be visible as much and is, presumably, mostly neglected in other work. Thus, the occurring mass transfer from the bubble into the liquid may be significantly underestimated. The extent to which the two opposing transport directions influence each other as well as the experimental evaluation must be clarified in more detail in further experiments.

In the rising-bubble test cell the same test systems have been applied to investigate the initial stages of the rapidly occurring volume change. The bubble rises through a static liquid. The contact time is shorter but the temporal resolution is higher because of the used cameras. This is particularly relevant for rapidly changing bubble sizes. Fig. 4 b displays measurements of initially pure CO_2 bubbles in degassed water. The initial volumes vary between 4 and 12 mm^3.

From the measured volume using the ideal gas equation

$$pV = NRT \tag{23}$$

with R as the universal gas constant and T as the temperature, the molar mass can be determined as a function of time. The influence of the hydrostatic pressure is corrected for every time step and according vertical position. In addition to the actual amount of substance, the surface area of the bubble is also known and the mass transfer coefficient can be determined by applying Eq. (15). The assumption is made that the surface concentration can be calculated by Henry's law, the bubble is ideally mixed, and the main mass transfer resistance is on the liquid side. The resulting mass transfer coefficients are presented in Fig. 5.

To compare the determined values with the literature, the values are represented in dimensionless quantities like the Reynolds and Sherwood number. In Fig. 6 a, the Sherwood number is given as a function of the Reynolds number. During the ascent, the rising velocity is changing as well as the bubble size. Since both of these values decline over time, the Reynolds number is decreasing as well. The results for three different initial diameters of CO_2 bubbles in water, as shown in Fig. 6 a, are

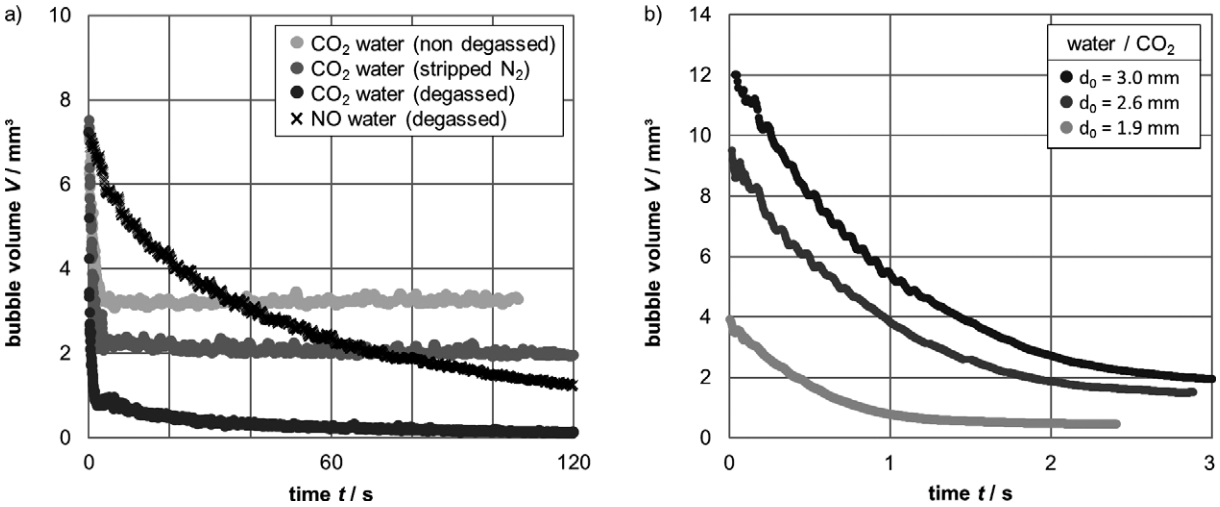

Figure 4. Bubble volume as a function of time (a) for three differently prepared continuous phases in the countercurrent-flow cell; (b) for three different initial bubble sizes of CO_2 in degassed water in the rising-bubble test cell.

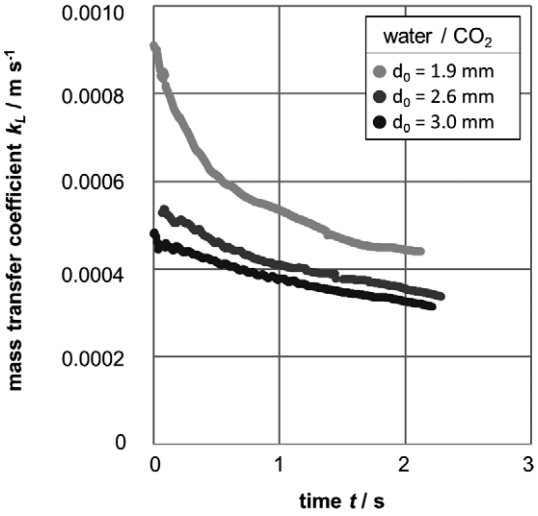

Figure 5. Mass transfer coefficient as function of time for CO_2 bubbles in degassed water with different initial diameter.

lying between the correlations given by Mersmann [2] and Brauer [3]. Despite the fact that an initially pure CO_2 bubble was inserted, a steady bubble size significantly larger than zero was observed after around 3 s. This indicates the existence of a different component which is initially transported into the bubble. This effect occurs despite prior degassing of the water.

To calculate the Sherwood numbers, the gas phase composition was adjusted over time. As a first assumption, the amount of the second component B inside the bubble was described with a constant molar flow:

$$N_{B,G} = t\,\dot{N}_B \tag{24}$$

until the experimentally determined constant bubble size is reached.

The same test systems applied in the countercurrent-flow cell. As an additional system NO/water is shown in Fig. 6 b. Although the volume decrease is significantly slower, the Sherwood numbers are comparable to that found for a CO_2 bubble due to the lower Henry's law solubility constant and smaller diffusivity in water shown in Sect. 2.3.

The values indicated in Fig. 6 b have been taken from the first few results of each measurement since the assumption of a pure gas bubble is most suitable during the initial stages of the experiment. As the amount of substance in the bubble diminishes, the composition changes because of the unavoidable mass transfer into the gas phase. Thus, the driving concentration difference at the interface is changing. The resulting Sherwood numbers in both experimental test rigs for small contact times are in good agreement, as can be seen in Fig. 6. There is a deviation for longer contact times. Until now, there is a lack of knowledge about the exact concentration development, which increases the difficulty to determine the Sherwood numbers for longer contact times. Hosoda et al. [4] attempted to describe the gas-phase composition for larger bubbles over time. However, there was not an almost degassed continuous phase but the concentrations of the dissolved components were known.

3.3 Mass Transfer in a System with Chemical Reaction

The results for the reactive system containing Fe^{II}(EDTA) with a concentration of $c_{FeII(EDTA)} = 75\ mmol\ L^{-1}$ in degassed water and NO as the gas phase are illustrated in Fig. 6 as well. The resulting Sherwood numbers are obviously higher than those of CO_2/water due to the mass transfer enhancement by the homogeneous chemical reaction. The dissolving NO is consumed by the reaction and thus, the driving concentration gradient is kept at a high level. It would be possible to influence the reac-

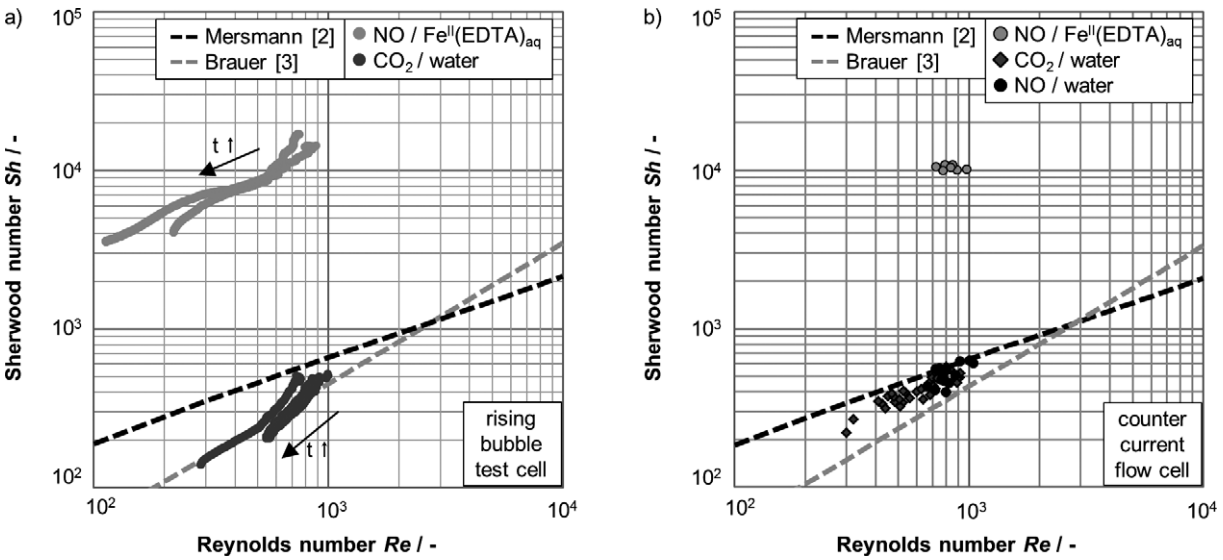

Figure 6. Sherwood number as function of Reynolds number for bubbles in degassed water and degassed water with $c_{FeII(EDTA)} = 75\ mmol\ L^{-1}$ (a) in the rising-bubble test cell; (b) at the beginning of the measurement in the countercurrent-flow test cell.

tion rate or the solubility of the NO by varying the temperature or the pressure. Another parameter that can be varied is the concentration of the educts in the liquid phase. In Fig. 7, different concentrations of Fe^{II}(EDTA) in degassed water are indicated. The lowest Sherwood numbers were found for the case of pure degassed water ($c_{FeII(EDTA)} = 0\,mmol\,L^{-1}$). In this case, the Sherwood number describes only the purely physical transport without reaction. As soon as a chemical reaction occurs in the liquid phase with the dissolving NO, the mass transfer is intensified and it can be described with the enhancement factor E, given in Eq. (13).

The factor depends on concentration and increases with rising educt concentration $c_{FeII(EDTA)}$. For the highest concentration of $c_{FeII(EDTA)} = 75\,mmol\,L^{-1}$, the enhancement factor E increases about 23-fold. An increase in the mass transfer and thus the enhancement factor E with increasing concentration meets the expectations and can be accurately measured with the system.

4 Conclusions

The aim of the study was the measurement of the mass transfer coefficient for systems where a homogeneous reaction in the liquid with a dissolving gas component occurs. Fluid dynamic investigations built a basis as these can be used to test the facility for its applicability. The terminal velocity of bubbles is a sensitive quantity for contamination. With the measurements of air bubbles in ultrapure water it was shown that the expected values can be measured with a high accuracy. Furthermore, the mass transfer experiments were carried out in different systems and experimental setups.

The results obtained for mass transfer of CO_2 and NO behave according to literature values. Particular attention must be paid, however, to the pretreatment of the continuously liquid phase. Depending on the amount of dissolved gases, differently strong volume reductions can be observed. Therefore, not only the mass transfer from the gas bubble into the liquid has to be taken into account but also transport from the continuous into the disperse phase. If this is not done, the occurring mass transfer of the dissolving component is significantly underestimated. To improve knowledge about the gas-phase composition, further investigations are necessary.

With the use of a chemical reaction to Fe^{II}(NO) in the liquid phase the enhancement of the mass transfer from single bubbles could be demonstrated. This effect which can be described by the enhancement factor, depends on the concentration $c_{FeII(EDTA)}$ which is consistent with the measurements. In addition to varying the concentration or other properties, the chosen reaction system offers the potential to directly influence the reaction rate by the choice of the ligands. It was proven that mass transfer coefficients and, therefore, Sherwood numbers can be determined under a controlled variation of chemical system, educt concentration, and bubble diameter.

Acknowledgment

This work is part of the Priority Program "Reactive bubbly flows". Financial support by the Deutsche Forschungsgemeinschaft (DFG SPP1740) is gratefully acknowledged (KR 1632/22-1).

The authors have declared no conflict of interest.

Symbols used

A	[m^2]	surface area
c	[$mol\,m^{-3}$]	molar concentration
d	[m]	diameter
D	[m^2s^{-1}]	diffusion coefficient
E	[–]	enhancement factor
f	[–]	dimensionless factor (Mersmann)

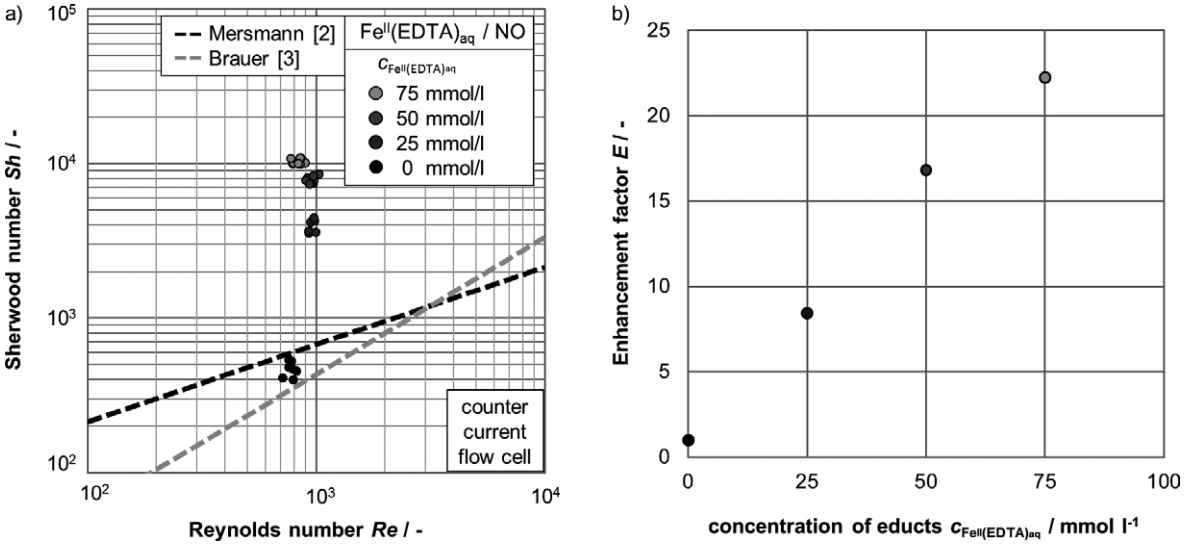

Figure 7. Countercurrent-flow test cell. (a) Sherwood number as function of the Reynolds number for different concentrations $c_{FeII(EDTA)}$ in degassed water; (b) enhancement factors as function of the educt concentration.

f_B	[s^{-1}]	bubble frequency
H	[mol $m^{-3}Pa^{-1}$]	Henry's law solubility constants
k	[m s^{-1}]	mass transfer coefficient
K_{NO}	[M^{-1}]	stability constants
$\dot{n}_i$	[mol $s^{-1}m^{-2}$]	molar flux
p	[Pa]	pressure
Pe	[–]	Péclet number, $\gamma\ d^2/D$
N	[mol]	amount of substance
R	[J $mol^{-1}K^{-1}$]	universal gas constant
Re	[–]	Reynolds number, $vd\rho/\mu$
Sc	[–]	Schmidt number, $\mu/(\rho D)$
Sh	[–]	Sherwood number, $k_L d/D$
Sr	[–]	Strouhal number, fBd/v
t	[s]	time
T	[K]	temperature
v	[m s^{-1}]	velocity
V	[m^3]	volume
x	[m]	x-coordinate, main flow direction
y	[m]	y-coordinate, normal to the probe surface
z	[m]	z-coordinate, perpendicular to the main flow direction

Greek letters

β	[–]	relative wall shear rate fluctuation amplitude
ζ	[–]	variable for the edge effect correction function
μ	[Pa s]	dynamic viscosity
ρ	[kg m^{-3}]	density

Sub- and superscipts

A	component A
B	component B
bulk	bulk
int	interfacial
G	gas
L	liquid
NO	reaction with NO
rea	reaction
tot	total

Abbreviation

px	pixel

References

[1] R. Clift, J. Grace, M. Weber, *Bubbles, Drops and Particles*, Academic Press, New York **1978**.

[2] A. Mersmann, *Stoffübertragung*, Springer Verlag, Berlin **1986**. DOI: 10.1007/978-3-642-82617-7

[3] H. Brauer, in *Fortschritte der Verfahrenstechnik*, VDI Verlag, Düsseldorf **1979**.

[4] S. Hosoda, S. Abe, S. Hosokawa, A. Tomiyama, *Int. J. Heat Mass Transfer* **2014**, *69*, 215–222. DOI: 10.1016/j.ijheatmasstransfer.2013.10.031

[5] J. Timmermann, M. Hoffmann, M. Schlüter, *Chem. Eng. Technol.* **2016**, *39 (10)*, 1955–1962. DOI: 10.1002/ceat.201600299

[6] A. Paschedag, W. Piarah, K. Schulze, M. Kraume, *WIT Trans. Model. Simul.* **2001**, *29*, 195–204. DOI: 10.2495/MB010191

[7] R. Higbie, *Trans. Am. Inst. Chem. Eng.* **1935**, *31*, 365–383.

[8] D. Rees, R. Palmer, S. Moncada, *PNAS* **1989**, *86 (9)*, 3375–3378.

[9] L. J. Ignarro, *Biosci. Rep.* **1999**, *19 (2)*, 51–71. DOI: 10.1023/A:1020150124721

[10] A. Franke, R. van Eldik, *Eur. J. Inorg. Chem.* **2013**, *(4)*, 460–480. DOI: 10.1002/ejic.201201111

[11] J. Chen, L. Wang, J. Zheng, J. Chen, *Bioprocess. Biosyst. Eng.* **2015**, *38 (7)*, 1373–1380. DOI: 10.1007/s00449-015-1378-7

[12] W. Li, J. Zhao, L. Zhang, Y. Xia, N. Liu, S. Li, S. Zhang, *Sci. Rep.* **2016**, *6 (18876)*, 1–10. DOI: 10.1038/srep18876

[13] N. Liu, Y. Jiang, L. Zhang, Y. Xia, B. Lu, B. Xu, W. Li, S. Li, *Energy Fuels* **2014**, *28 (12)*, 7591–7598. DOI: 10.1021/ef5014852

[14] H. Niu, D. Leung, *Environ. Rev.* **2010**, *18*, 175–189. DOI: 10.1139/A10-007

[15] C. de Salas, M. Heinrich, *Green Chem.* **2014**, *16*, 2982–2987. DOI: 10.1039/c3gc42432d

[16] P. van der Maas, L. Harmsen, S. Weelink, B. Klapwijk, P. Lens, *J. Chem. Technol. Biotechnol.* **2004**, *79 (8)*, 835–841. DOI: 10.1002/jctb.1057

[17] Y. Xia, J. Zhao, M. Li, S. Zhang, S. Li, W. Li, *Environ. Sci. Technol.* **2016**, *50 (7)*, 3846–3851. DOI: 10.1021/acs.est.5b05861

[18] Y. Xia, Y. Shi, Y. Zhou, N. Liu, W. Li, S. Li, *Energy Fuels* **2014**, *28 (5)*, 3332–3338. DOI: 10.1021/ef500604d

[19] S. Zhang, W. Li, C. Wu, H. Chen, Y. Shi, *Appl. Microbiol. Biotechnol.* **2007**, *76*, 1181–1187. DOI: 10.1007/s00253-007-1078-6

[20] S. Zhang, H. Chen, Y. Xia, N. Liu, B. Lu, W. Li, *Appl. Microbiol. Biotechnol.* **2014**, *98 (20)*, 8497–8512. DOI: 10.1007/s00253-014-6016-9

[21] T. Schneppensieper, S. Finkler, A. Czap, R. van Eldik, M. Heus, P. Nieuwenhuizen, C. Wreesmann, W. Abma, *Eur. J. Inorg. Chem.* **2001**, *2*, 491–501. DOI: 10.1002/1099-0682(200102)2001:2<491::AID-EJIC491>3.0.CO;2-2

[22] T. Schneppensieper, A. Wanat, G. Stochel, S. Goldstein, D. Meyerstein, R. van Eldik, *Eur. J. Inorg. Chem.* **2001**, *9*, 2317–2325. DOI: 10.1002/1099-0682(200109)2001:9<2317::AID-EJIC2317>3.0.CO;2-F

[23] T. Schneppensieper, A. Wanat, G. Stochel, R. van Eldik, *Inorg. Chem.* **2002**, *41 (9)*, 2565–2573. DOI: 10.1021/ic011220w

[24] B. Aas, P. Klüfers, *Eur. J. Inorg. Chem.* **2017**, in press. DOI: 10.1002/ejic.201601330

[25] M. Wolf, P. Klüfers, *Eur. J. Inorg. Chem.* **2017**, in press. DOI: 10.1002/ejic.201601329

[26] R. Sander, *Chem. Phys.* **2015**, *15 (8)*, 4399–4981. DOI: 10.5194/acp-15-4399-2015

[27] M. Frank, J. Kuipers, W. van Swaaij, *J. Chem. Eng. Data* **1996**, *41*, 297–302. DOI: 10.1021/je950157k

[28] I. Zacharia, W. Deen, *Ann. Biomed. Eng.* **2005**, *33 (2)*, 214–222. DOI: 10.1007/s10439-005-8980-9

